

Featureless and Non-Fractionalized Bose Insulator on the Honeycomb Lattice at $1/2$ site-filling

Itamar Kimchi,¹ S. A. Parameswaran,¹ Ari M. Turner,^{1,2} and Ashvin Vishwanath^{1,3}

¹*Department of Physics, University of California, Berkeley, CA 94720, USA*

²*Institute for Theoretical Physics, University of Amsterdam,
Valckenierstraat 65, 1018 XE Amsterdam, The Netherlands*

³*Materials Science Division, Lawrence Berkeley National Laboratories, Berkeley, CA 94720*

(Dated: July 4, 2012)

It is well known that band insulators require an integer number of electrons (of each spin) per unit cell. Similarly, in bosonic insulators where the number of particles per unit cell (f) is fractional, the ground state either enlarges the unit cell, or realizes an exotic topologically ordered (fractionalized) state. Symmetric non-fractionalized Mott insulators only appear at integer f . However, the converse problem is relatively unexplored - is such a symmetric non-fractionalized insulator always allowed at integer f , or can it be prohibited by other lattice symmetries? An especially relevant example is the honeycomb lattice - where free spinless fermions at $f = 1$ (or, $1/2$ site filling) are always metallic, due to point group symmetries. Here we argue that bosons at the same filling however can realize a Mott phase. We propose a wave function for this state and by a mapping to a classical partition function we compute its properties and demonstrate that the state is insulating, fully symmetric and has no topological order. Thus the absence of symmetry breaking in this case does not imply topological order. Our construction suggests that featureless insulators are generically allowed for bosons at unit filling on any symmorphic lattice in any dimension.

Within the Landau paradigm, phases of matter are distinguished by spontaneous symmetry breaking. Implicit here is the assumption that a completely symmetric state (a paramagnet, in the context of spin systems) exists. In classical systems, this is just the high temperature phase. However, when discussing quantum phases at zero temperature, a paramagnetic state could be forbidden. For example, according to the Lieb-Schultz-Mattis¹ theorem, for the spin- $\frac{1}{2}$ Heisenberg antiferromagnet in one dimension, no completely symmetric quantum paramagnet exists. A spin disordered state with exponentially decaying spin correlations will necessarily break lattice symmetries. An extension of this theorem² applies to two dimensions. In the square lattice spin- $\frac{1}{2}$ Heisenberg model, which has a half-odd-integer spin per unit cell, the spin disordered phase is not a trivial paramagnet. If it does not break lattice symmetries then it must be a quantum spin liquid, which has a hidden form of order called topological order. The latter leads to fractionalized excitations with novel statistics, and is distinct from our notion of a featureless paramagnet. The absence of symmetry breaking can then be taken as indirect confirmation of the quantum spin liquid, which is often used as a diagnostic both in numerics and in experiments³. Furthermore, in these systems where a trivial paramagnet is forbidden, quantum phase transitions often lie outside the Landau-Ginzburg-Wilson paradigm⁴. Therefore it is important to understand exactly when such trivial paramagnets are disallowed.

These considerations can be readily translated to boson systems in a periodic lattice⁵, as realized by ultracold atomic gases in optical lattices⁶. We assume a homogeneous system, and the *filling* is defined as the number of bosons per unit cell. When the filling is not an integer, the ground state must break some symmetry, eg.

by forming a superfluid or enlarging the unit cell, or, by realizing a topologically ordered state. On a simple lattice with say one site per unit cell, a Mott insulating state can appear at integer filling of bosons⁵. This is the bosonic analog of the trivial paramagnet. In a simple caricature of this state, each site is occupied by a fixed integer number of bosons. Clearly such a caricature does not work on more complicated lattices, with more than a single site per unit cell. For example, we can ask whether a lattice with $n > 1$ equivalent sites per unit cell can exhibit an insulating phase at a filling of one boson per unit cell. In some cases the lattice can be broken down into non-overlapping sets of finite number of sites, or molecules, which preserve all the symmetries, and can be considered as providing a single orbital at integer filling. However, for lattices like the kagome and honeycomb with $n = 3, 2$ respectively, no finite grouping of disconnected sites retains the symmetries of the lattice. In this case it is less obvious how to construct a Mott state at unit filling (which corresponds to $1/3$ and $1/2$ boson per site respectively). One possibility is to consider a topologically ordered phase where emergent excitations carry a fraction of the boson charge, which can then be placed at integer site filling. However as we argue below, in these two situations and in several others, a fully symmetric non-fractionalized Mott insulator is possible. Throughout this paper, we consider only *tight-binding* models where particles are restricted to occupy sites on the given lattice. This is crucial to distinguish between the triangular, honeycomb and kagome lattices, which share the same space group symmetries.

In a recent publication⁷ we demonstrated that a symmetric and non-fractionalized Mott Insulator could be constructed on the kagome lattice at filling one per unit cell. This was accomplished by obtaining a family of ex-

ponentially localized Wannier orbitals that respect lattice symmetries, and occupying each one with a boson. This construction requires that a band insulator of spinless fermions can also be defined at the same filling, since a Slater determinant of these Wannier orbitals produces a band insulator.

While a band insulator is possible at unit filling on the kagome lattice, it is known that (spinless) fermions on the honeycomb lattice are always gapless at filling one per unit cell (which corresponds to half a fermion per site). This is relevant to the band structure of graphene, which is gapless at the corners of the Brillouin zone ($\pm\mathbf{K}$ points), but also holds for more general tight binding Hamiltonians. The lattice symmetries of rotation and reflection ensure that the two bands touch at these points. In this case our previous construction⁷ is not applicable. In fact, one may suspect that the absence of a free fermion band insulator on this lattice may indicate that no fully symmetric bosonic insulator exists either. In this case, this would be a model which, even at integer unit cell filling, is prohibited from realizing a trivial insulating phase.

However, we show that a separate wave function, which we term the Voronoi permanent, can be constructed on the honeycomb lattice and shown to have the desired properties i.e. it is an insulating wave function with the right filling, without either symmetry breaking or topological order. Our key idea is simple - we construct a molecular orbital involving equal superposition of the six sites of the honeycomb, and insert one boson in each of these orbitals. The resulting wave function is a permanent of single particle wave functions that involve sites within the Voronoi unit cell (sites closest to the center of each hexagon), hence the term *Voronoi permanent*. Since sites are shared between hexagons, deducing properties of this state requires further calculation. We show this wave function can be mapped to a two dimensional statistical mechanical problem of loops, whose properties are calculated using Monte Carlo simulations. The result indicates that we have a fully symmetric and non-fractionalized Mott phase on the honeycomb lattice.

Recently, a interesting numerical study of the honeycomb lattice Hubbard model with spin 1/2 fermions has appeared⁸. A phase at intermediate coupling appears to be insulating and spin gapped but without symmetry breaking of any kind, and was proposed to be a spin liquid with topological order. While this conclusion may ultimately be correct, and though the states we propose are not directly candidate wave functions with SU(2) spin symmetry, they are sufficiently similar that one may suspect that spin symmetric paramagnets may also exist on the honeycomb lattice, and may be an alternate explanation of these results. Positive signatures of a quantum spin liquid such as ground state degeneracy or topological entanglement entropy⁹⁻¹¹ should settle this question.

We note that our method can be extended to any symmorphic lattice, where the point group symmetries and the translations are independently generated, to con-

struct a candidate Mott state at unit filling. However for non-symmorphic lattices our method fails since we cannot identify a symmetric unit cell. At this point we may ask — is there any lattice on which a symmetric non-fractionalized Mott insulator is forbidden at integer filling? While we do not have a definitive answer to this question, we note that non-symmorphic lattices are promising candidates. Familiar non-symmorphic lattices include the diamond and pyrochlore lattices.

This paper is structured as follows. We begin by demonstrating the unique difficulties of constructing insulators on the honeycomb lattice, thus motivating our work. Next we explain our construction of the Voronoi permanent state, a candidate wavefunction for a featureless bosonic insulator, and proceed to show that its correlations can be understood in terms of a classical loop model. We describe the simulation of this loop model using a Monte Carlo worm algorithm, and use this to show that the state describes a symmetric insulating phase on the honeycomb lattice. We close with a discussion of the relevance of our results for quantum spin systems and extensions to other symmorphic lattices.

I. FREE FERMIONS AND HONEYCOMB LATTICE SYMMETRIES

Consider spinless *fermions* on the honeycomb lattice. The nearest-neighbor tight-binding model yields a spectrum with Dirac points at the $\pm\mathbf{K}$ points of the Brillouin zone, where two dispersing bands touch. At half-filling with one fermion per unit cell, the lower band is occupied and the Fermi energy is at the Dirac points. In order to gap out a Dirac point, a lattice symmetry (reflection, threefold rotation or inversion) must be spontaneously broken. In fact the band touching at the $\pm\mathbf{K}$ points holds beyond the Dirac limit, for any tight binding Hamiltonian on this lattice. To see this, we study the irreducible representations of the ‘little group’ of the Dirac points. At any momentum \mathbf{q} in the Brillouin zone, the little group $G_{\mathbf{q}}$ is the subgroup of the space group that leaves \mathbf{q} invariant or translates it by a reciprocal lattice vector; the Bloch Hamiltonian $h_{\mathbf{q}}$ at \mathbf{q} commutes with the little group generators and so we can classify energy bands using irreducible representations of $G_{\mathbf{q}}$.

Consider the \mathbf{K} point; our arguments apply equally well to $-\mathbf{K}$. Rotations by $2\pi/3$ leave \mathbf{K} invariant, so the generator of threefold symmetry $R_{2\pi/3} = R_{\pi/3}^2$ is in the little group. The other little group generator is the mirror reflection σ_2 – which also leaves \mathbf{K} invariant – and together these generate $G_{\mathbf{K}} \cong D_{3h}$. These generators act on the two components of the Bloch function which represent the amplitudes to be on the two sublattices of the honeycomb. Their representation matrices take the form

$$R_{2\pi/3} = \begin{pmatrix} e^{i2\pi/3} & 0 \\ 0 & e^{-i2\pi/3} \end{pmatrix}, \quad \sigma_2 = \begin{pmatrix} 0 & 1 \\ 1 & 0 \end{pmatrix}$$

These form a two-dimensional irreducible representation, and thus the band touching is protected by symmetry. This argument carries through for spinful fermions with $SU(2)$ spin rotation symmetry in which case half-filling corresponds to two fermions per unit cell. Thus, there is no fermionic band insulator at half-filling on the honeycomb lattice that preserves all its symmetries.

It was recently demonstrated that in some cases one can construct bosonic quantum Mott insulating wavefunctions given the orthogonal, symmetric, and exponentially localized Wannier orbitals of a fermionic band insulator at the same filling⁷. For the honeycomb, the protection of the band touchings by symmetry forbids the existence of Wannier orbitals that satisfy these criteria, and thus this approach fails. We therefore need an alternate construction which we discuss below.

II. CANDIDATE HONEYCOMB MOTT STATE

Consider the honeycomb lattice with one boson per unit cell. Since this corresponds to half a boson per site, we cannot construct a featureless insulator by restricting bosons to individual sites. The next option is to delocalize bosons across some supercell. However, any choice of non-overlapping supercells necessarily breaks symmetry. We could attempt to construct linear combinations of symmetric supercells that are orthogonal while preserving the symmetry, but these would be symmetric Wannier orbitals which would not be exponentially localized because of the band touching on the honeycomb noted above. Instead, we use the smallest supercell that preserves the lattice symmetry, corresponding to the six sites of a hexagon. Neighboring hexagons have overlapping sites; this complication arises for any choice of supercell. This motivates the following ‘hexagon product state’,

$$|\Psi_{\square}\rangle = \prod_{\mathbf{R}} B_{\mathbf{R}}^{\dagger} |0\rangle \quad (1)$$

$$B_{\mathbf{R}}^{\dagger} \equiv \frac{1}{\sqrt{6}} \sum_{j \in \square_{\mathbf{R}}} b_j^{\dagger}. \quad (2)$$

Here j labels a site and \mathbf{R} a unit cell, i.e. a site on the Bravais lattice, $\square_{\mathbf{R}}$ denotes the sites on hexagonal plaquette centered at \mathbf{R} , and $|0\rangle$ is the boson vacuum. In first quantized form, the wavefunction is

$$\Psi_{\square}(\mathbf{r}_1, \mathbf{r}_2, \dots, \mathbf{r}_N) = \text{perm}[\phi_{\mathbf{R}_i}(\mathbf{r}_j)] \quad (3)$$

where $\phi_{\mathbf{R}}(\mathbf{r}) = \langle 0 | b_{\mathbf{r}} B_{\mathbf{R}}^{\dagger} | 0 \rangle$, and perm refers to the permanent¹². Note that since each hexagon is in one-to-one correspondence with a unit cell, and each unit cell has two sites, this state has the requisite $1/2$ boson per site. Since they are permanents of bosonic orbitals¹³ defined on a symmetric Voronoi cell of the lattice, we term such wavefunctions *Voronoi permanents*.

The key to this Voronoi permanent construction is to associate with each unit cell a single-particle orbital

which preserves all point group symmetries. This is possible on *symmorphic* lattices, for which all the symmetries may be realized at a single point, as we elaborate below. For example, a similar hexagon state on the kagome lattice corresponds to $1/3$ boson per site, since each unit cell has three sites.

The expression (1) for $|\Psi_{\square}\rangle$ is more complicated than it would appear at first sight. Because hexagons on neighboring unit cells overlap, it is a highly entangled state. Such quantum entangled states have no classical analogue and are difficult to visualize. More to the point, because of the nonorthogonality of the hexagons we cannot tell whether $|\Psi_{\square}\rangle$ describes a featureless insulator, a superfluid or another symmetry broken state. This requires an explicit computation, to which we now turn.

III. MAPPING $|\Psi_{\square}\rangle$ TO A LOOP MODEL

We wish to study properties of $|\Psi_{\square}\rangle$ such as the boson correlation function:

$$G^{bos}(i, j) = \frac{\langle \Psi_{\square} | b_i^{\dagger} b_j | \Psi_{\square} \rangle}{\langle \Psi_{\square} | \Psi_{\square} \rangle}. \quad (4)$$

which describes the ability of the particles to propagate between lattice sites i and j . In a Mott insulator, this decays exponentially, while for a 2D superfluid at $T = 0$ it exhibits long range order. Actually as we demonstrate below we can map the correlations in $|\psi_{\square}\rangle$ to those of a classical finite temperature 2D model with short-range interactions. True long-range order is thus ruled out by the Mermin-Wagner theorem. Correlations must decay at least algebraically, corresponding to a Kosterlitz-Thouless (KT) superfluid phase. The only other possible ordering is a discrete breaking of lattice symmetry, which can be diagnosed by studying the spatial structure of correlations. Topological order is ruled out for this state since it is an unconstrained product state.

Relating the ground-state wavefunction to Boltzmann weights of a classical statistical mechanical model has notable precedents including the Laughlin fractional quantum Hall wavefunction¹⁴, the Rokhsar-Kivelson wavefunction of dimer models^{15,16} and the AKLT spin wavefunction^{17–20}. In our case there are different ways to represent G^{bos} in terms of a classical partition function. The first involves the statistical mechanics of closed loops on the triangular lattice, and since it offers multiple advantages it will be our primary tool. A second approach (described in the supplementary material) is based on coherent states of bosons, and was used to benchmark loop model results.

We begin by showing that the normalization $\langle \Psi_{\square} | \Psi_{\square} \rangle$ is the partition function of the loop model derived below. Following the definition of $|\Psi_{\square}\rangle$ we have

$$\langle \Psi_{\square} | \Psi_{\square} \rangle = \langle 0 | \left(\prod_{\mathbf{R}} B_{\mathbf{R}} \right) \left(\prod_{\mathbf{R}'} B_{\mathbf{R}'}^{\dagger} \right) | 0 \rangle, \quad (5)$$

where the products are over sites \mathbf{R} of the (triangular) Bravais lattice. By commuting $B_{\mathbf{R}}$, $B_{\mathbf{R}}^{\dagger}$ past each other,

we find that the correlation function is mapped to a sum over products of commutators in which each $B_{\mathbf{R}}$ operator is matched with one $B_{\mathbf{R}}^\dagger$ operator,

$$\langle \Psi_\square | \Psi_\square \rangle = \sum_{\sigma} \prod_{\mathbf{R}} [B_{\mathbf{R}}, B_{\sigma(\mathbf{R})}^\dagger] \quad (6)$$

where σ denotes a permutation of the sites on the triangular lattice. Since only neighboring hexagons share sites, the commutator is

$$[B_{\mathbf{R}}, B_{\mathbf{R}'}^\dagger] = \delta_{\mathbf{R}, \mathbf{R}'} + m \delta_{\mathbf{R}', \text{nn}(\mathbf{R})} \quad (7)$$

where $\text{nn}(\mathbf{R})$ denotes the nearest neighbors of \mathbf{R} on the Bravais lattice. Here $m = \frac{1}{3}$ ($m = \frac{1}{6}$) for the honeycomb (kagome) lattice. In general, $m = p/q$ where p is the number of sites shared by a pair of neighboring Voronoi cells, each of which has q sites. For a hexagonal Voronoi cell $q = 6$, and $p = 2(1)$ for the honeycomb (kagome) lattice.

Using (7) we can restrict the sum over permutations in (6) to those in which each site is matched with either (i) itself, contributing a multiplicative factor of 1 to the weight (which we represent as an empty site), or (ii) a neighboring site, contributing a factor m (which we represent as an arrow pointing from B to B^\dagger). Since every site must be matched to exactly one other site, the arrows form closed loops which cannot intersect or touch; a loop of length L contributes a multiplicative factor of m^L to the partition sum. *Thus, the normalization defines a statistical mechanical model of closed, nonintersecting directed loops (which we take to include empty sites and dimers) on the triangular lattice, in which each loop segment contributes a multiplicative weight m to the probability of a given configuration.* The inclusion of empty sites and dimers, and the constraint that loops cannot intersect (or touch), distinguish this particular loop model from more conventional ones studied.

A similar argument relates the numerator of (4) to a defect correlator of this loop model: the b^\dagger and b operators each remove one of the B and B^\dagger operators respectively, giving a pair of defects, a site with an arrow out but no arrow in and its converse. Thus each configuration contributing to the numerator must include a single open loop.

This interpretation as a loop model unifies the states on all lattices with the same underlying Bravais lattice. For the triangular Bravais lattice, the physical states on the kagome and honeycomb appear as specific points in the continuum of possible values for the loop weight m . For an intuitive understanding of the meaning of this continuum of values, consider decorating the honeycomb lattice by adding a site (represented by $a_{\mathbf{R}}^\dagger$) to the center of each hexagon, and modify the definition of $B_{\mathbf{R}}^\dagger$,

$$B_{\mathbf{R}}^\dagger \rightarrow \cos \theta a_{\mathbf{R}}^\dagger + \frac{\sin \theta}{\sqrt{6}} B_{\mathbf{R}}^\dagger \quad (8)$$

Since only b sites are shared by hexagons, computing the commutator now yields (7) with $m = \frac{1}{3} \sin^2 \theta$ on the

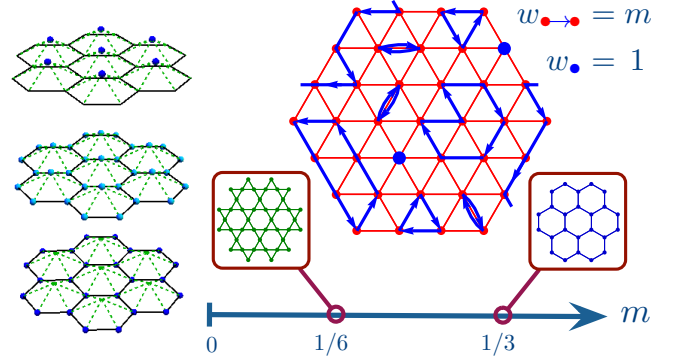


FIG. 1: Voronoi construction and loop mapping
(L) Decorated honeycomb and delocalization of bosons onto hexagons as in Eq. (8); m increases from 0 to $1/3$ from top to bottom. (R) Sample loop configuration showing loops, dimers and empty sites which do not touch or intersect. Below we show the continuum of loop weights m , where $m = 0$ is the atomic insulator and $m = 1/6, 1/3$ correspond to Voronoi permanents on the kagome and honeycomb.

honeycomb. For $\theta = 0$, we have an atomic insulator, since the bosons are restricted to the central site. As we increase θ we spread bosons across hexagons until we arrive at the ‘honeycomb point’ $\theta = \pi/2$ ($m = 1/3$) where we can remove the empty central site. We have sketched this construction of the Voronoi permanent in Fig. 1.

Thus, the mapping to the loop model lets us interpolate from the atomic ($m = 0$) limit to the honeycomb ($m = 1/3$) point as shown schematically in Fig. 1. This interpolation allows us to study the evolution of the correlation functions from the atomic insulator limit at $m = 0$ where the correlation length vanishes.

We compute correlation functions of the loop model using a modified classical Monte Carlo worm algorithm²¹. The worm algorithm is especially suited to this problem because it works naturally with the loop representation and as noted previously, breaking continuous symmetry in the model yields a KT superfluid with algebraically decaying correlations. First, unlike most approaches the worm algorithm is not expected to exhibit critical slowing down in the algebraic phase. Second, it can often access large system sizes more efficiently than alternative approaches. Third, knowledge of the worm winding numbers allows us to directly compute the helicity modulus (proportional to the superfluid density), a definitive diagnostic of the KT phase²². This vanishes in the disordered phase and exhibits a universal jump of $\frac{2}{\pi}$ at the KT transition²³. More complicated superfluid orders (e.g. a ‘pair superfluid’ where $\langle (b_i^\dagger)^2 \rangle \neq 0$ but $\langle b_i^\dagger \rangle = 0$) will also be captured in this approach.

We performed extensive worm algorithm Monte Carlo simulations for periodic $L \times L$ triangular lattice systems, with $L = 12, 16, 20$, and averaged over 10^6 Monte Carlo steps per site (MCS) in each case (10^5 MCS were sufficient for the kagome at low $m = 1/6$). Each system was

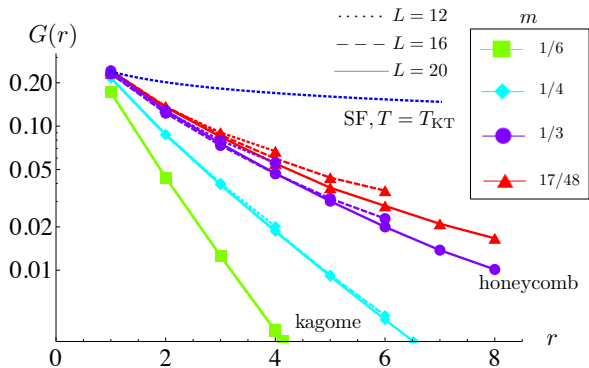


FIG. 2: **Loop model correlation function.**

Linear-log plot with distance measured along a basis vector. The fastest possible KT algebraic decay, $\sim r^{-1/4}$, is shown for comparison; $m = 1/3$ (corresponding to the honeycomb lattice) displays exponential decay, indicating an insulating phase. Error bars are smaller than the line widths.

initialized in the ‘ $m = 0$ ’ configuration with no loops, and allowed to equilibrate over 50 000 MCS before recording averages. Error estimates were obtained by computing the standard error of the data from 20 independent runs, a conservative approach. We benchmarked results against coherent state simulations at $m = 1/3, 1/6$ and loop perturbation theory at small m^{24} and found excellent agreement. Our results are summarized in Figs. 2, 3 and 4.

IV. NUMERICAL RESULTS

We study the properties of the honeycomb state in two distinct ways. First, we focus directly on the honeycomb lattice. In addition to computing the correlation function and winding numbers (hence, the superfluid density) in the loop representation using the worm algorithm (at $m = 1/3$), we also compute the correlation function for smaller system sizes directly using a coherent state representation of the honeycomb wavefunction (see the supplement for details). In addition, we determine whether any discrete symmetry is broken by explicitly checking that the correlations preserve all lattice symmetries²⁵. Second, we enlarge the study to include other points on the m axis, including $m = 1/3$ for the honeycomb, $m = 1/6$ for the kagome, $m = 1/4$ as an intermediate state and $m = 17/48$ which lies beyond the honeycomb point. We use the worm algorithm to study the evolution of the superfluid density and the correlation function from the trivial $m = 0$ atomic insulator to the $m = 1/3$ honeycomb and even slightly beyond.

We find that $G^{bos}(i, j)$ decays exponentially with a correlation length of $\xi \sim 2.4$ lattice sites, as shown in Fig. 2. The correlation length evolves from $\xi = 0$ at $m = 0$ to $\xi \sim 0.9$ lattice sites at the kagome ($m = 1/6$) and remains a small fraction of the system size for m values beyond the honeycomb. As is clear from Fig. 2, the

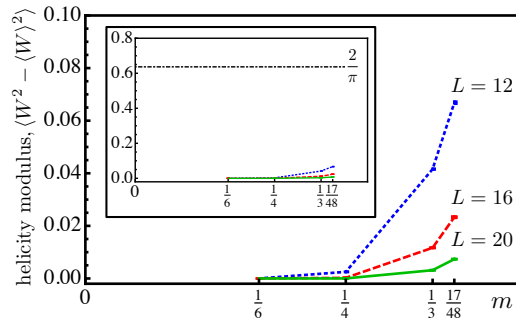


FIG. 3: **Helicity modulus.**

The helicity modulus (proportional to the superfluid density) tends to zero for increasing L , consistent with the expectation from KT finite-size scaling for the insulating phase. (Inset) Same figure, with axes zoomed out to show that the helicity moduli for all m values studied are much smaller than the universal value of $2/\pi$ at the KT transition (the smallest superfluid density allowed in the KT phase). Error bars are smaller than the markers.

correlations decay exponentially and cannot be fit by a power law. We also plot for comparison the most rapid possible algebraic decay in the KT phase, $G(r) \sim r^{-1/4}$, to emphasize that algebraic decay of single boson correlations is ruled out from this analysis.

As shown in Fig. 3, the superfluid densities are all much less (see inset) than the universal jump value $2/\pi$ at the KT transition²³, indicating that the wavefunction remains in the insulating phase for the m values studied. Multi-boson condensates are also ruled out by this observation. As expected, we find that smaller system sizes overestimate the superfluid order, and the superfluid density decreases with increasing size, consistent with the claim that the honeycomb Voronoi permanent describes an insulating state.

Finally, neither the loop model nor the coherent state simulations exhibit breaking of discrete lattice symmetries for the honeycomb lattice Voronoi permanent. To determine this, short MC runs were used to avoid averaging out any symmetry-breaking by oversampling. As an example, a 500 MCS coherent boson run for $L = 12$ gave rms values of symmetry-breaking of less than 2% of the maximum. As a simple visual demonstration of lattice symmetry, a sample correlation function for the loop model on the triangular lattice at $m = 1/3$ from an $L = 12$, 500 MCS worm algorithm run is shown in Fig. 4. Details of the analysis are provided in the supplementary material.

V. EXTENSIONS TO OTHER LATTICES

Our construction of a candidate symmetric Mott insulator wave function at unit filling can be extended to any symmorphic lattice, where a primitive unit cell that respects all lattice symmetries is present (the Voronoi cell

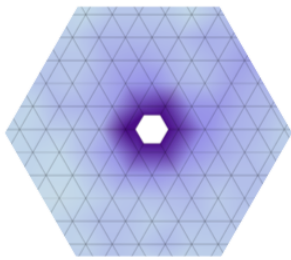


FIG. 4: **Lattice symmetries in the correlation function.**

Interpolated contour plot of loop model correlation function at $m = 1/3$, with white space in the center corresponding to the central peak. Correlations decay rapidly and are consistent with lattice symmetries.

for example). Imagine introducing a site at the center of the unit cell and filling it with one boson (the atomic insulator). Then, gradually transfer the boson to the physical sites in the unit cell thereby obtaining a family of wave functions controlled by one parameter as in Eq.(8). This family of wavefunctions has a loop model description defined on the underlying Bravais lattice. When the added sites are fully depleted they can be detached to yield the desired Voronoi permanent wave function. The loop model description of the state can then be used to check whether the Voronoi permanent lies in the same phase as the atomic insulator, using techniques similar to those in this paper. Symmorphic lattices in any dimension thus always admit the construction of Voronoi permanents. Determining if the state is ordered must be done on a case-by-case basis. Here we described the most basic construction — more complicated wave functions with additional tuning parameters could be constructed on similar lines, which could expand the range of available states.

Another 2D example is the checkerboard lattice with two sites in the unit cell, which may be viewed as a set of corner sharing tetrahedra in two dimensions. Again, the (spinless) fermionic bands must touch due to lattice symmetries²⁶. However, our Voronoi permanent construction could be applied here too. An example in $d = 3$ is the cubic perovskite lattice of corner-sharing octahedra (Fig 5) with three sites per unit cell. Here fermions are again gapless at filling one per unit cell but the Voronoi permanent construction applies here as well. Another 2D example with a band touching was considered in Ref. 27, but in this case it is trivial to construct a Bose insulator by filling non-overlapping sets of sites.

On non-symmorphic lattices it is impossible to choose a unit cell that respects all the space group symmetries (or alternatively, to choose a unique symmetric point at which to place the decorated site) and the construction fails. Examples of non-symmorphic lattices include the well known pyrochlore and diamond lattices.

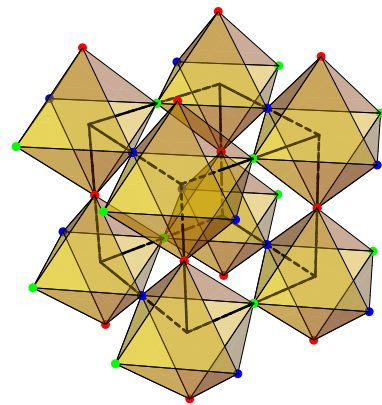


FIG. 5: **Corner sharing octahedron lattice**

This is a symmorphic lattice with sites at the vertices of corner-sharing octahedra. A Voronoi permanent wavefunction of a candidate insulating state at unit cell filling of one (corresponding to $1/3$ site filling) can be constructed.

VI. DISCUSSION

We began this paper by posing a question: is a featureless and non-fractionalized (i.e., topologically trivial) insulating phase possible for a system of bosons on the honeycomb lattice at a filling of one boson per unit cell? By explicitly constructing a simple trial wavefunction and computing correlations within it, we have argued that this is indeed the case: the Voronoi permanent wavefunction we proposed captures the essential properties of such a featureless insulating phase. The honeycomb is an especially interesting example, because its free fermion band structure cannot be insulating without breaking symmetry. As a corollary, we found that a similar wavefunction on the kagome lattice — which can be viewed as the truncation of wavefunctions of Ref. 7 — also represents an insulating phase. If we attempt to make a Slater determinant of the honeycomb lattice Voronoi orbitals, the state vanishes. However, a similar procedure on the kagome lattice is expected to lead to a band insulating state of fermions which is allowed by symmetry.

In both cases the wave functions obtained are positive definite, and could be ground states of an unfrustrated bosonic model. Here, we have not discussed Hamiltonians for which these are ground states. However, general methods to construct parent Hamiltonians for wave functions like those discussed here — which are captured by partition functions of local statistical mechanical models — have been discussed by Henley²⁸. Furthermore, recently ultracold atoms have been confined to kagome²⁹ and honeycomb³⁰ optical lattices. This motivates the study of realistic Mott-Hubbard model Hamiltonians which could potentially realize such fractional site filling insulators. Both these directions are left to future work.

Our wave function can also be interpreted as a spin

wave function where different boson occupations are different S_z values, and only $U(1)$ spin rotation about the z axis is a symmetry. The honeycomb lattice wave function then represents a featureless magnetization plateau at $2/3$ of the saturation value, with $S = 3/2$ spins on the sites. We can also write down a wave function for $S = 1/2$ by projecting out multiple boson occupation from our state (hardcore limit). This state is appropriate for a $U(1)$ symmetric spin system, and, if projection does not modify its basic properties, it represents a spin gapped $S_z = 0$ state on the honeycomb lattice without topological order. The effect of projection must be checked numerically, but is expected to further suppress superfluid correlations and not affect the topological properties, although it may enhance lattice symmetry breaking effects.

Our approach is readily extended to all symmorphic lattices, where analogues of the hexagon product state can be immediately constructed. While numerical checks are required to confirm these are states with the desired properties, these are straightforward since they reduce to classical statistical mechanics of loops. We note that it is not even possible to construct such promising candidates for bosons at fractional unit cell filling. This suggests that the unit filling of symmorphic lattices is an essentially different situation, where symmetric non-fractionalized Mott states are generically allowed.

We note however that our method fails for non-symmorphic lattices, which include interesting examples such as the diamond and pyrochlore lattices. We speculate that a fully symmetric non-fractionalized bosonic Mott state is absent on such lattices, even at a filling of one boson per unit cell.

ACKNOWLEDGEMENTS

We thank Olexei Motrunich, Bryan Clark, Tarun Grover, Matthias Troyer, and Shivaji Sondhi for useful discussions, and Dan Stamper-Kurn for collaboration on related work. This research is supported in part by the NSF under Grant No. DGE 1106400 (IK), the Simons Foundation (SAP) and the Army Research Office with funding from the DARPA Optical Lattice Emulator program (AV).

SUPPLEMENTARY MATERIAL

1. Loop Model Mapping

Let us recapitulate the mapping from the quantum boson correlator to the statistical mechanical loop model in more detail. For both the kagome and honeycomb lattices, it is convenient to explicitly decompose the coordinate $i \equiv (\mathbf{R}, \alpha)$ where α is a sublattice index and $\mathbf{R} = m\mathbf{a}_1 + n\mathbf{a}_2$ is a point on the triangular Bravais lattice,

with \mathbf{a}_1 and \mathbf{a}_2 primitive lattice vectors (shown in the figure) and we define for future reference $\mathbf{a}_3 = -(\mathbf{a}_1 + \mathbf{a}_2)$. We wish to compute the boson correlation function

$$G_{\alpha, \alpha'}^{bos}(\mathbf{R}, \mathbf{R}') = \langle b_{\mathbf{R}, \alpha}^\dagger b_{\mathbf{R}', \alpha'} \rangle \quad (9)$$

within the hexagon product state/Voronoi permanent

$$|\Psi_\square\rangle = \prod_{\mathbf{R}} \left(\sum_{\mathbf{R}', \alpha} f_{\mathbf{R}}(\mathbf{R}', \alpha) b_{\mathbf{R}', \alpha}^\dagger \right) |0\rangle. \quad (10)$$

For the kagome lattice, $\alpha = 1, 2, 3$ where we choose a symmetric unit cell in which the three sites belonging to a unit cell lie in the directions of the primitive Bravais lattice vectors $\mathbf{a}_1, \mathbf{a}_2, \mathbf{a}_3$ respectively. For the hexagon state we then have $f_{\mathbf{R}}(\mathbf{R}', \alpha) = \frac{1}{\sqrt{6}} (\delta_{\mathbf{R}, \mathbf{R}'} + \delta_{\mathbf{R}, \mathbf{R}' + \hat{\mathbf{e}}_\alpha})$ where the final $\hat{\mathbf{e}}_\alpha$ refers to the Bravais lattice vector pointing from one hexagon to an adjacent hexagon which shares sublattice site α with it. For our choice of unit cell, $\hat{\mathbf{e}}_\alpha = \mathbf{a}_\alpha$.

For the honeycomb, $\alpha = 1, 2$ where the unit cell is taken to consist of the two sites on a vertical bond. For the hexagon state we then have $f_{\mathbf{R}}(\mathbf{R}', \alpha) = \frac{1}{\sqrt{6}} (\delta_{\mathbf{R}, \mathbf{R}'} + \delta_{\mathbf{R}, \mathbf{R}' - \mathbf{a}_1} + \delta_{\mathbf{R}, \mathbf{R}' + \mathbf{v}_\alpha})$ where we define $\mathbf{v}_1 = \mathbf{a}_3$ and $\mathbf{v}_2 = \mathbf{a}_2$.

Again we begin with the normalization (i.e. the denominator of (4))

$$\langle \Psi_\square | \Psi_\square \rangle = \langle 0 | \left(\prod_{\mathbf{R}} B_{\mathbf{R}} \right) \left(\prod_{\mathbf{R}'} B_{\mathbf{R}'}^\dagger \right) |0\rangle \quad (11)$$

with $B_r^\dagger = \sum_{\mathbf{R}', \alpha} f_{\mathbf{R}}(\mathbf{R}', \alpha) b_{\mathbf{R}', \alpha}^\dagger$.

A single pair $B_{\mathbf{R}'}^\dagger, B_{\mathbf{R}}$ gives the commutator $C[\mathbf{R}, \mathbf{R}'] = \sum_{\mathbf{R}_1, \mathbf{R}_2, \alpha_1, \alpha_2} f_{\mathbf{R}}(\mathbf{R}_1, \alpha_1) f_{\mathbf{R}'}(\mathbf{R}_2, \alpha_2)$. In a Wick type decomposition, this becomes a sum over all bijective (one-to-one) maps i.e. permutations $\sigma : \mathbf{R} \rightarrow \mathbf{R}'$, with each term in the sum being the product of commutators $\prod_{\mathbf{R}} C[\mathbf{R}, \sigma(\mathbf{R})]$. We are saved from computing this functional integral because the hexagons of two unit cells overlap only if they belong to the same or neighboring unit cells, $C[\mathbf{R}, \mathbf{R}'] = \delta_{\mathbf{R}, \mathbf{R}'} + m\delta_{\mathbf{R}', nn[\mathbf{R}]}$, so maps σ only appear in the sum if they take \mathbf{R} either to itself (weight 1) or to a neighbor (weight m).

Making contact with the description in the main text, an allowed map σ can be pictured as a collection of arrows between neighboring sites on the triangle lattice, with each site \mathbf{R} either having no arrows (in case σ maps it to itself) or exactly one arrow going out (to $\sigma(\mathbf{R})$) and one arrow coming in (to $\sigma^{-1}(\mathbf{R})$). Therefore $\langle \Psi_\square | \Psi_\square \rangle$ is a sum over directed closed loop configurations on the triangle lattice, with each configuration in the sum weighted by m to the power of the total length of its loops. Loops may not touch or intersect with the exception of the zero area length two loop, which is permitted. Strictly speaking this is gives generalized vertex model (with 37 states per vertex, 6^2 two-in-two-out states and one for the case when the site is mapped to itself) and not a simple loop

model, though we may still study it by the worm algorithm by incorporating two bond-occupation flavors. We are interested in $m = 1/6$ and $m = 1/3$, corresponding to the kagome and honeycomb lattices respectively.

Next, we turn to the numerator. Each b operator knocks out a B operator with a coefficient f , resulting in a sum over *defect correlators*,

$$G_{\alpha,\alpha'}^{bos}(\mathbf{R}, \mathbf{R}') = \sum_{\mathbf{R}_1, \mathbf{R}_2} f_{\mathbf{R}_1}(\mathbf{R}, \alpha) f_{\mathbf{R}_2}(\mathbf{R}', \alpha') G^{worm}(\mathbf{R}_1, \mathbf{R}_2) \quad (12)$$

where we named the defect correlator G^{worm} because of its natural interpretation as a correlation function in the worm algorithm for $\mathbf{R}_1 \neq \mathbf{R}_2$,

$$G^{worm}(\mathbf{R}_1, \mathbf{R}_2) = \frac{\langle 0 | \left(\prod_{\mathbf{R} \neq \mathbf{R}_1} B_{\mathbf{R}} \right) \left(\prod_{\mathbf{R}' \neq \mathbf{R}_2} B_{\mathbf{R}'}^\dagger \right) | 0 \rangle}{\langle \Psi_\square | \Psi_\square \rangle}. \quad (13)$$

For the kagome, the boson correlator is given by the sum of four worm correlator values; for the honeycomb, the sum of nine. Thus, we can extract correlation functions on the honeycomb and kagome lattices explicitly from the worm algorithm defect correlator.

2. Loop Perturbation Theory

Within first-order perturbation theory in m , loops are costly and the sum in the numerator will involve only configurations where the defects are connected by the shortest line segment between them. To this order, restricting for a moment to a 1D lattice, we find that defect configurations are all multiplied by an extra factor of $c^{|R-R'|}$. This naive estimate holds when there is only one shortest line connecting the defects, as is the case when $R - R'$ is a multiple of a triangle lattice vector R_1 or R_2 . However, consider the case where $R - R' = n(R_1 + R_2)$. Then there are many shortest line segments between the defects, identical to the number of shortest paths between opposite corners of an n by n square lattice. There are $\binom{2n}{n}$ such paths, asymptotically going as $4^{|R-R'|}$. Thus we find that the asymptotic behavior of the correlation function is

$$\langle b_0^\dagger b_\ell \rangle \sim (4m)^\ell$$

within first order perturbation theory in $m \sim 1/T$. This perturbation theory result turns out to overestimate the extent of the algebraically decaying superfluid phase. However, it provided a further benchmark of the worm algorithm computation of the loop model correlation function.

3. Worm algorithm calculations

The directed loop configurations with and without an open loop may be studied simultaneously using a Monte

Carlo ‘worm’ algorithm²¹. The basic idea of the worm algorithm is to simultaneously gather statistics on the correlation function and the normalization in (4) by working directly in the loop representation. The ‘worm’ is an open loop configuration; by allowing a worm to shrink or grow by a random process, until it closes of its own accord while preserving detailed balance – implemented by a local-update Metropolis algorithm – one gains statistics on both open and closed configurations, which contribute respectively to the numerator and denominator of (4). The canonical example of the use of a worm algorithm is to study the XY model in the loop-current (dual) representation.

Unlike the usual XY case, our loop model has strong interactions in that the loops are forbidden to touch or intersect, necessitating some modifications to the algorithm. Here, we merely note that the twin complications of loop self-avoidance and the triangular lattice geometry presents unique challenges for the worm algorithm. Specifically, at higher values of m when long loops are relatively favorable, the worm can occasionally get ‘stuck’ in a configuration (for instance, a spiral) for which nearly all proposed updates will be rejected. To extricate the worm from such a configuration requires exponentially many update steps and thus the correlation function is poorly sampled and the algorithm fails to converge. This issue necessitated long runs ($\gtrsim 10^6$ MCS) for the honeycomb, though for smaller m we found 10^5 MCS to be sufficient. For the honeycomb ($m = 1/3$) a single run at the largest system size ($L = 20$) did not converge even after 10^9 updates; we discarded it and a similar $m = 17/48$ run when taking averages. We note that the honeycomb data for $L = 12, 16$ are free of such convergence issues.

4. Additional Numerical Data

In Fig. 6 we show a log-log plot of the worm algorithm correlation function to a power law for the largest system size, $L = 20$ (same data as in Fig. 2) with the fastest KT algebraic decay shown for comparison on a log-log plot. It is clear that a power-law fit is inconsistent with the data as this would appear as a straight line on this plot.

5. Helicity Modulus in Terms of Winding Numbers

The relation between worm winding numbers and the helicity modulus may be seen as follows. Take the loop model on a torus and thread a flux θ through one of its handles, say the cycle associated with the periodic boundary condition $\vec{r} \sim \vec{r} + L\hat{x}$ in the \hat{x} direction. This is equivalent to a uniform vector potential $A\hat{x}$ permeating the system with magnitude $A = \theta/L$. The Boltzmann factor for the worm to grow a step $\delta\vec{R}$ now appears multiplied by the phase $\exp(iA\hat{x} \cdot \delta\vec{R})$. This phase factor cancels out for any closed loop, *unless it threads the torus*, crossing the periodic boundary conditions with a

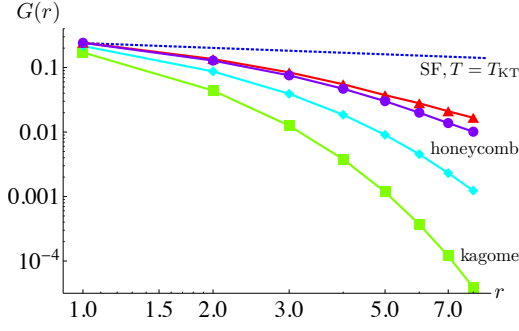


FIG. 6: **Loop model correlation function.**

Log-log plot as a function of distance along a basis vector, demonstrating power-law fit is impossible. Error bars smaller than linewidths.

nonzero *winding number* $W_x \equiv \int \hat{x} \cdot \delta \vec{R} / L$. The winding number is integer-valued for closed loops. Let W_x stand for the sum of all \hat{x} winding numbers in a given closed loop configuration. Then the free energy owing to the flux, $\Delta F[\theta] = F[\theta] - F[0]$ is given by

$$\exp(-\beta \Delta F[\theta]) = \langle \exp(i\theta W_x) \rangle \quad (14)$$

yielding the helicity modulus

$$Y \equiv d^2 F / d\theta^2|_{\theta=0} = \beta^{-1} (\langle W^2 \rangle - \langle W \rangle^2). \quad (15)$$

The superfluid inverse temperature β which appears in these expressions is set to 1 in our model. Studying winding number fluctuations (or, the combination βY) thus allows us to identify the transition point.

6. Bosonic Coherent States

Another way to map the wavefunction $|\Psi_\square\rangle$ is to work in the basis of bosonic coherent states. Let us consider the bosonic correlation function,

$$G^{bos}(0, j) = \langle b_0^\dagger b_j \rangle = \delta_{j0} + \frac{\langle \Psi_\square | b_j b_0^\dagger | \Psi_\square \rangle}{\langle \Psi_\square | \Psi_\square \rangle} \quad (16)$$

We now use the resolution of identity for bosonic coherent states,

$$\mathbf{1} = \int [dz_i d\bar{z}_i] e^{-\sum_i |z_i|^2} |\{z_i\}\rangle \langle \{z_i\}| \quad (17)$$

where $|\{z_i\}\rangle = \otimes_i |z_i\rangle$ and $[dz_i d\bar{z}_i] = \prod_i \frac{d\text{Re} z_i d\text{Im} z_i}{\pi}$. Inserting this above, and using the property of the coherent

states that $b_i |\{z_i\}\rangle = z_i |\{z_i\}\rangle$ and $\langle 0 | \{z_i\} \rangle = 1$ we find

$$\langle b_0^\dagger b_j \rangle = \delta_{j0} + \frac{\int [dz_i d\bar{z}_i] e^{-\sum_i |z_i|^2} \prod_{\mathbf{R}} |\mathcal{B}_{\mathbf{R}}(z)|^2 (z_j \bar{z}_0)}{\int [dz_i d\bar{z}_i] e^{-\sum_i |z_i|^2} \prod_{\mathbf{R}} |\mathcal{B}_{\mathbf{R}}(z)|^2} \quad (18)$$

where $\mathcal{B}_{\mathbf{R}}(z) = \sum_i f_{\mathbf{R}}(i) z_i$. We see that it suffices to consider the correlation function $\langle z_{\mathbf{R}} \bar{z}_0 \rangle$ of the statistical mechanical model described by a complex number at each site, with the manifestly positive semi-definite Boltzmann weight $\mathcal{P}(\{z_i\}) = \prod_{\mathbf{R}} |\mathcal{B}_{\mathbf{R}}(z)|^2 e^{-\sum_i |z_i|^2}$.

As the model has only $U(1)$ symmetry (as is evident from the form of the wavefunction), even in two dimensions it can exhibit an algebraically correlated KT phase, and so the worm algorithm Monte Carlo on the loop model is a more convenient tool to study the phase. Nevertheless, the coherent boson approach can be readily simulated using a simple local-update Metropolis algorithm which allows us to benchmark the worm results on small system sizes. We find excellent agreement between the worm and coherent boson results through the largest system size studied with the latter algorithm, $L = 12$.

7. Discrete Symmetry Breaking

The worm algorithm explicitly computes the correlation functions of the boson order parameter, and we are able to conclude that there is no long-range superfluid order. However, this does not immediately rule out discrete symmetry-breaking which could occur via an Ising transition. To study this from the correlation function, it is convenient to work with the correlation function $G_{\alpha\beta}^{bos}(\mathbf{R}) \equiv \langle b_{\mathbf{R},\alpha}^\dagger b_{0,\beta} \rangle$ from the site $0, \beta$ to the site \mathbf{R}, α where as before we label the sites by their Bravais lattice vector and sublattice index. If we now perform a discrete (i.e. point-group) symmetry operation U on the lattice, we have in general that $G_{\alpha\beta}^{bos}(\mathbf{R}) \rightarrow U G_{\alpha\beta}^{bos}(\mathbf{R}) U^{-1}$ with the operator U transforming both the site index as well as possibly the sublattice indices. We may define the ‘Ising’ order parameter corresponding to symmetry U as

$$\mathcal{I}_{\alpha\beta}^{(U)}(\mathbf{R}) \equiv G_{\alpha\beta}^{bos}(\mathbf{R}) - U G_{\alpha\beta}^{bos}(\mathbf{R}) U^{-1} \quad (19)$$

and by explicitly examining the correlation functions we can verify that this vanishes asymptotically within our error estimates. In the main text we quote the rms average of $\mathcal{I}_{\alpha\beta}^{(U)}(\mathbf{R})$. We perform this test explicitly for mirror reflections and rotations that together generate the lattice point group. For these symmetry breaking tests we use short Markov chains of 100 – 2000 MCS, to ensure that the chains do not sample multiple symmetry broken states while still collecting sufficient statistics for computing the order parameter. To check for symmetry breaking we primarily used simulations of the wavefunctions in the coherent state representation, since fluctuations in the associated Markov chains exhibit shorter correlations than those in the worm algorithm.

-
- ¹ E. Lieb, T. Schultz, and D. Mattis, *Annals of Physics* **16**, 407 (1961).
 - ² M. B. Hastings, *Phys. Rev. B* **69**, 104431 (2004).
 - ³ L. Balents, *Nature* **464**, 199 (2010).
 - ⁴ T. Senthil, A. Vishwanath, L. Balents, S. Sachdev, and M. P. A. Fisher, *Science* **303**, 1490 (2004).
 - ⁵ M. P. A. Fisher, P. B. Weichman, G. Grinstein, and D. S. Fisher, *Phys. Rev. B* **40**, 546 (1989).
 - ⁶ M. Greiner, O. Mandel, T. Esslinger, T. W. Hansch, and I. Bloch, *Nature* **415**, 39 (2002).
 - ⁷ S. A. Parameswaran, I. Kimchi, A. M. Turner, D. M. Stamper-Kurn, and A. Vishwanath, *ArXiv e-prints* (2012), arXiv:1206.1072 [cond-mat.str-el].
 - ⁸ Z. Y. Meng, T. C. Lang, S. Wessel, F. F. Assaad, and A. Muramatsu, *Nature* **464**, 847 (2010).
 - ⁹ T. Grover, *ArXiv e-prints* (2011), arXiv:1112.2215 [cond-mat.str-el].
 - ¹⁰ H.-C. Jiang, Z. Wang, and L. Balents, *ArXiv e-prints* (2012), arXiv:1205.4289 [cond-mat.str-el].
 - ¹¹ S. Depenbrock, I. P. McCulloch, and U. Schollwoeck, *ArXiv e-prints* (2012), arXiv:1205.4858 [cond-mat.str-el].
 - ¹² The permanent of an $n \times n$ matrix A_{ij} is defined as $\text{perm}(A_{ij}) = \sum_{\sigma} \prod_{i=1}^n A_{i,\sigma(i)}$, where the sum extends over all permutations σ of n objects, i.e. it is like a determinant without the alternating sign.
 - ¹³ We note that permanent wavefunctions have been considered for magnetization plateaus on the anisotropic triangular lattice by T. Tay and O. Motrunich, *Phys. Rev. B* **81**, 165116 (2010).
 - ¹⁴ R. B. Laughlin, *Phys. Rev. Lett.* **50**, 1395 (1983).
 - ¹⁵ D. S. Rokhsar and S. A. Kivelson, *Phys. Rev. Lett.* **61**, 2376 (1988).
 - ¹⁶ R. Moessner and S. L. Sondhi, *Phys. Rev. Lett.* **86**, 1881 (2001).
 - ¹⁷ I. Affleck, T. Kennedy, E. H. Lieb, and H. Tasaki, *Phys. Rev. Lett.* **59**, 799 (1987).
 - ¹⁸ I. Affleck, T. Kennedy, E. H. Lieb, and H. Tasaki, *Commun. Math. Phys* **115**, 477 (1988).
 - ¹⁹ D. P. Arovas, A. Auerbach, and F. D. M. Haldane, *Phys. Rev. Lett.* **60**, 531 (1988).
 - ²⁰ S. A. Parameswaran, S. L. Sondhi, and D. P. Arovas, *Phys. Rev. B* **79**, 024408 (2009).
 - ²¹ N. Prokof'ev and B. Svistunov, *Phys. Rev. Lett.* **87**, 160601 (2001).
 - ²² The superfluid density is directly related to fluctuations in the winding number W , which counts worms that wind around a torus loop.
 - ²³ D. R. Nelson and J. M. Kosterlitz, *Phys. Rev. Lett.* **39**, 1201 (1977).
 - ²⁴ Supplementary Material.
 - ²⁵ For this purpose we used short Monte Carlo runs to avoid sampling different broken-symmetry states.
 - ²⁶ K. Sun, H. Yao, E. Fradkin, and S. A. Kivelson, *Phys. Rev. Lett.* **103**, 046811 (2009).
 - ²⁷ H. Yao and S. A. Kivelson, *Phys. Rev. Lett.* **105**, 166402 (2010).
 - ²⁸ C. L. Henley, *Journal of Physics: Condensed Matter* **16**, S891 (2004).
 - ²⁹ G.-B. Jo, J. Guzman, C. K. Thomas, P. Hosur, A. Vishwanath, and D. M. Stamper-Kurn, *Phys. Rev. Lett.* **108**, 045305 (2012).
 - ³⁰ L. Tarruell, D. Greif, T. Uehlinger, G. Jotzu, and T. Esslinger, *Nature* **483**, 302 (2012).